Modeling Wear of Journal Bearings

P. Bergmann [*1], F. Grün[1]
[1]Montanuniversität Leoben, Department Product Engineering
*Franz-Josef-Straße 18, A-8700 Leoben, philipp.bergmann@unileoben.ac.at

Abstract: Wear in hydrodynamic journal bearings resulting from solid contact in the mixed friction regime becomes an increasingly prominent topic leading to the necessity of numerical wear evaluations. A numerical method tackling this topic based on Archard's wear law is presented and applied on a close-to-component journal bearing test rig. This approach allows a validation of numerical results by comparing them with resolved test results. The results illustrate the effects of solid contact on the process of wear chronologically and locally resolved. The subsequent influence of wear on fluid film geometry and pressure build up is presented. The numerical method proofs its usability to handle wear caused by solid contact in lubricated systems.

Keywords: Tribology, Hydrodynamic journal bearings, Mixed friction, Wear

1. Introduction

Due to actual legislative regulations for automotive industry implying a cap of average 95 g CO_2/km for an OEM's fleet by 2020 an overall increase of vehicles' efficiency is necessary [1]. Areas which offer a high potential to achieve this ambitious goal include light weight design, downsizing and the reduction of frictional losses by the use of low and ultra low viscosity oils as well as hybridization in connection with the start-stop technology. Having a look on hydrodynamic journal bearings in internal combustion engines these measures lead to increased specific loads and imply hindered operation conditions. Hydrodynamic journal bearings typically comprise of a steel shaft, a softer multilayer journal bearing shell and the lubricant, see fig.1. The relative motion between shaft and journal bearing results in a fluid film gap geometry allowing a hydrodynamic pressure build up. The resultant force F_{hyd} is in equilibrium with the external load F_{ext}. Dependent on load, rotational speed and viscosity respectively temperature the operational point of a journal bearing can be situated in fluid, mixed or boundary friction

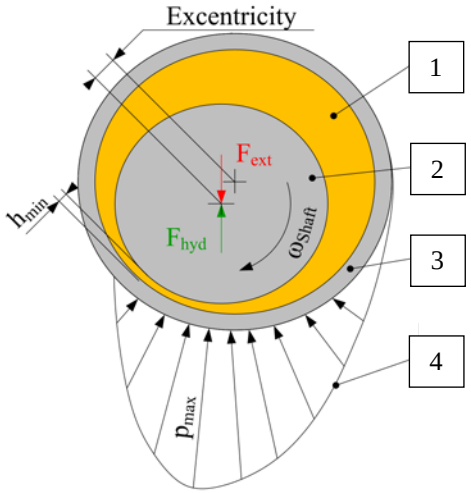

Figure 1: Scheme of a hydrodynamic journal bearing.

regime. This relation can be visualized with the help of a Stribeck curve, see fig. 2. The conventional area of operation is generally set in fluid friction regime in which both surfaces are completely separated by a lubrication film. The external load is completely carried by the resultant hydrodynamic pressure.

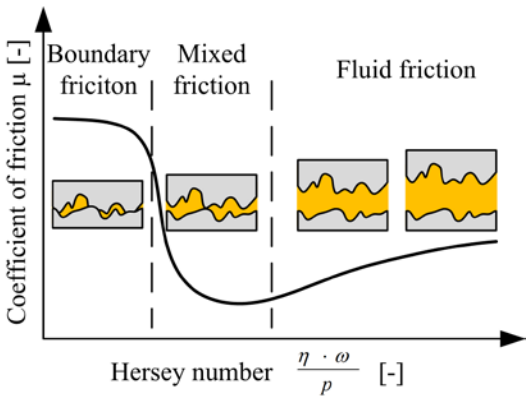

Figure 2: Principle Stribeck curve.

Actual developments, however, involve a reduction of the hydrodynamic carrying capacity resulting in lower fluid film thicknesses. Consequently surface asperities between shaft and bearing shell start to contact each other. In

this case hydrodynamic journal bearings operate in mixed and boundary friction regime which is characterized by the coexistence of hydrodynamic and solid contact pressure. The consequences of solid contact are increased frictional losses and wear limiting life expectancy - making a numerical wear assessment necessary [2-4].
The numerical calculation of lubricated systems uses the hydrodynamic fluid film theory according to Reynolds, which provides a differential equation to solve for the hydrodynamic pressure based on conducted experiments by Tower [5]. In simulations dealing with lubricated contacts solid contact is considered with the help of a load-displacement curve. Dependent on the local separation of both surfaces which equals the fluid film thickness this curve yields the solid contact pressure. Greenwood and Williamson were the first who investigated this topic and proposed an elastic model based on material and statistical surface parameters of the contacting surfaces [6]. An exemplary load-displacement curve representing the resulting solid contact pressure is depicted in fig. 3.

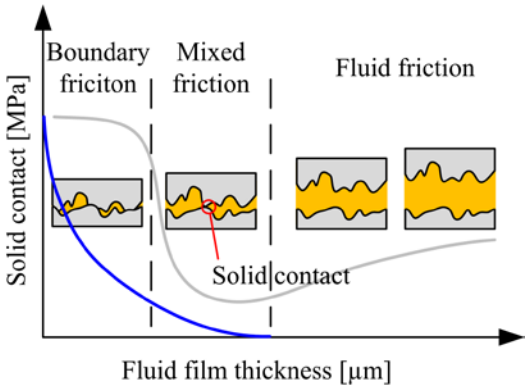

Figure 3. Principle contact model: load-displacement curve representing solid contact occurring in mixed and boundary friction regime.

At high film thicknesses which occur in the fluid friction regime the fluid film gap is large enough to separate the mating surfaces. With decreasing film thickness the gap between both surfaces reaches the order of surface asperities leading to solid contact which follows the function in fig.3. The field of wear assessment in COMSOL Multiphysics® has been addressed by several authors. Elabbasi suggests a time dependent wear equation based on Archard's wear law [7]. This equation represents an ordinary differential equation (ODE) and can be implemented in COMSOL Multiphysic® straightforwardly. The wear method was applied on a model representing a pin-on-disc wear test and validated with the help of test results. The resulting wear height was directly coupled within the established contact between pin and disc. The author further extended the method allowing the prediction of wear in an automotive disc brake. Sutton et al. developed a wear model using COMSOL Multiphysics® and LiveLink™ for MATLAB® also based on a modified Archard's wear law allowing locally resolved wear evaluations. Numerical evaluations were performed on a ball-on-flat reciprocating contact and validated by experiments [8]. Brown et al. investigated wear of a brake [9]. A wear rate model was implemented with the help of an ODE in the same manner as described in [7]. Using temperature-wear data the wear height was calculated chronologically and locally resolved. With the help of this approach it was possible to clarify the origin of a damage case.
So far presented work dealt with numerical wear evaluation in dry contacts directly coupling wear calculation and solid contact and illustrated the usability of this approach. The present paper, however, describes the application of the modified Archard's wear law on lubricated systems connected with arbitrary occurrent solid contact. The method was applied on a close-to-component test rig allowing an evaluation between numerical and real part investigations. Since the focus of this paper is the numerical wear approach necessary parameters were chosen following the goal to be able visualizing interesting aspects of the wear method and do not relate necessarily to real application parameter values.

2. Description of the test rig

The model under investigation involves the core parts of a close-to-component test rig combining a rotationary tribometer TE92HS from Phoenix Tribology and a journal bearing adapter (JBA), see fig. 4, a). The journal bearing specimen (I) is mounted in the specimen holder (II) which is further connected to the adapter, see fig. 4, c). As depicted in fig. 4, b) the journal bearings are pushed against a rotating shaft

specimen, which is connected to the drive shaft of the tribometer. An oil bath provides oil supply and can be heated. The specimen adapter is loaded by a lever mechanism which increases the given force of an air bellow. A multitude of measurement variables allow high sensible frictional and wear investigations enabling the comprehensive empirical derivation of wear coefficients which are crucial parameters for the numerical evaluation of wear [10].

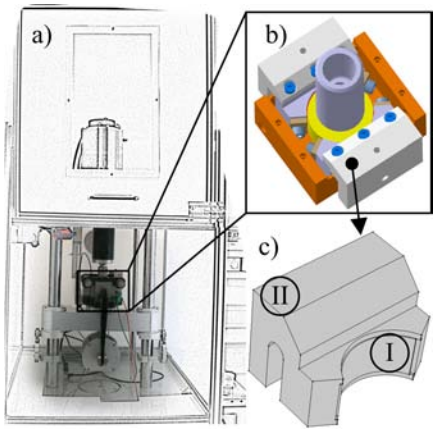

Figure 4: a) tribological test rig TE92HS combined with a journal bearing adapter, b) CAD depiction of the core parts, c) numerical model abstraction.

3. Use of COMSOL Multiphysics® Software

Solving this tribological wear problem requires the Solid Mechanics interface taking account of elastic deformation and solving equation (1) in combination with the Thin-Film Flow, Shell interface based on Reynolds' equation (2) in time-dependent notation. Equation (3) represents the modified form of Archard's wear law and is implemented with the help of a Boundary ODE.

$$\rho \frac{\partial^2 u}{\partial t^2} = \nabla u \cdot S + F_V \quad (1)$$

$$\frac{\partial}{\partial t}(\rho h) + \nabla_t \cdot (\rho h v_{av}) = 0 \quad (2)$$

$$\frac{\partial h_w}{\partial t} = p \cdot C \cdot v \quad (3)$$

The core parts of the above described test rig is set up in COMSOL Multiphysics® by assuming the model boundaries at the interface between specimen holder and the surrounding adapter. To take this into account roller conditions were set at boundary A, B and C, see fig. 5. The external load is implemented as a boundary load acting on boundary D. On boundary E Thin-Film Flow, Shell is applied yielding the hydrodynamic pressure p_{hyd}. The shaft specimen, however, can be considered as rigid due to its high stiffness in comparison to the bearing shell and specimen adapter. Subsequently the shaft is not modelled and only considered as shaping geometry of the fluid film. The resulting p_{hyd} is applied as Boundary Load in the Solid Mechanics module. Dependent on the resulting fluid film thickness the contact model yields a locally resolved contact pressure which is applied on boundary E as well and is used by the wear equation to calculate the resulting wear height h_w. h_w is further directly coupled with the Thin-Film Flow, Shell to take the changing geometry due to wear into account in the fluid film height.

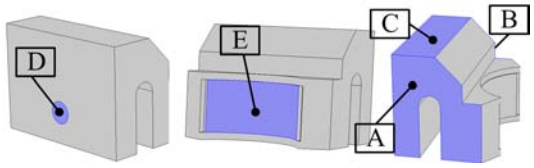

Figure 5: Numerical model set up. Boundary A, B and C: model boundaries. Boundary D: application of external load. Boundary E: area of acting hydrodynamic, solid contact pressure and wear height.

4. Numerical Scenarios

To investigate the usability of this numerical approach two situation were constructed. Scenario 1 was designed to clarify if the developed wear evaluation methodology takes wear due to solid contact into account properly. Since the resulting wear pattern affects the fluid film gap geometry and consequently the hydrodynamic pressure build up it was necessary to directly connect the occurring wear height pattern to the fluid film gap. Scenario 2 was designed to evaluate this connection.

4.1 Scenario 1

A sequence was set up putting the journal bearing system alternating into mixed and fluid friction by changing the hydrodynamic load carrying capacity using speed, see fig. 6. Starting

from an initially unloaded system the external force F_{ext} is raised linearly until the maximum force of 1500 N is reached. The sliding speed v remains constant during this phase. After the loading stage Stribeck cycles are performed starting at 100 s. Within 5 seconds the speed is ramped up to 1.2 m/s then reduced to 1e-5 m/s again while keeping the external load constant.

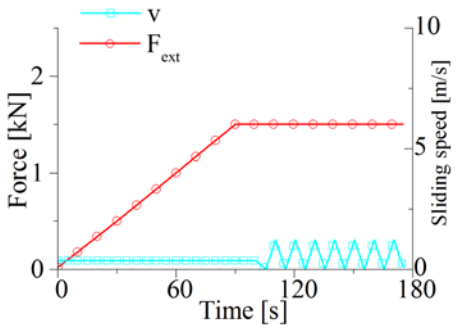

Figure 6. Run of the input parameters external load F_{ext} and sliding speed v of scenario 1.

4.2 Scenario 2

The investigation of the proper connection between wear height and fluid film gap can be properly examined when external parameters are kept constant and changes in resultant quantities origin from calculated data. Therefore the system was transferred from an initially hydrodynamic operation into a constant mixed friction regime. Starting from an operational point in fluid friction regime at F_{ext}=1000 N and a sliding speed of 12.6 m/s the speed is reduced linearly to 0.33 m/s within 100 seconds and kept constant for the remaining time. Fig. 7 depicts the chosen input parameters of scenario 2.

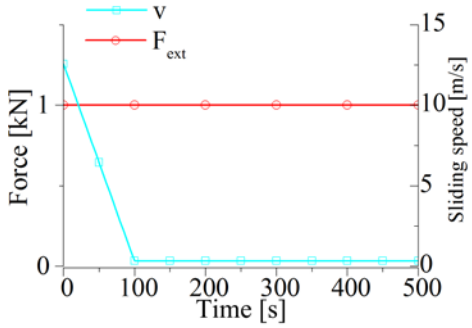

Figure 7. Run of the input parameters external load F_{ext} and sliding speed v of scenario 2.

5. Results

This section starts with a visualization of the resulting quantities illustrating the interplay between the specimen holder and acting pressures and forces. Afterwards the results of the chosen scenarios are presented.
Fig.8 illustrates an exemplary stress state of the deformed specimen holder subjected to the external load. The resulting hydrodynamic and solid contact pressure act on the bearing shell's surface leading to local stress concentrations.

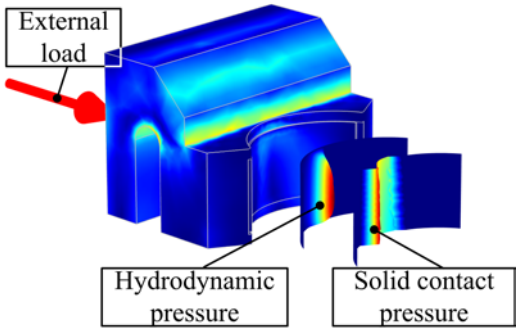

Figure 8: Model of test rig part under external load in mixed friction regime operation (hydrodynamic + solid contact pressure).

5.1 Results of Scenario 1

Fig. 9 depicts the time dependent run of the resulting quantities of scenario 1: the resulting hydrodynamic force F_{hyd}, the solid contact force $F_{contact}$ and the wear volume V_{wear}. Starting from an unloaded system the increasing F_{ext} is carried by F_{hyd} solely with progressive time.

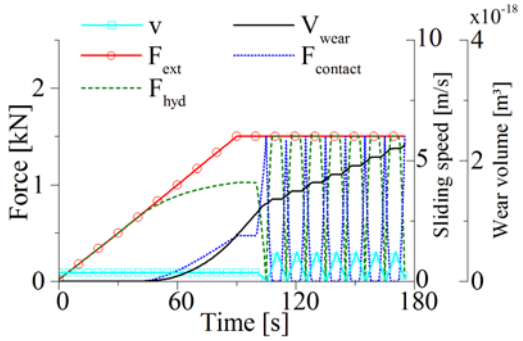

Figure 9: Resulting force equilibrium and wear volume run of scenario 1.

At 40 seconds the solid contact force starts to contribute to the force equilibrium and also starts to rise until the external load reaches its maximum value. Together with the contact force a rise of the wear volume sets in. At 100 seconds start-stop cycles begin. With decreasing sliding speed the contact force starts to contribute to an increasing extend until at speeds around 1e-5 m/s the external load is fully carried by the solid contact load. With increasing speed the hydrodynamic force starts to contribute increasingly while the solid contact force decreases until at speeds of 0.73 m/s the contact force totally vanishes and the external load is carried by F_{hyd} further on. At times when $F_{contact}$ acts, the wear volume increases while staying at a constant level when only the hydrodynamic force acts.

5.2 Results of scenario 2

At the initial state the external load is fully carried by the hydrodynamic force, see fig. 10. With decreasing rotational speed the carrying share changes and the solid contact force comes into play at 70 seconds. Simultaneously the onset of the wear volume occurs, comparable to scenario 1. At 100 seconds the system is set into the desired mixed friction regime. From this time on the external parameters F_{ext} and v are kept constant. With increasing time the contact force sinks while the wear volume and the hydrodynamic force rise.

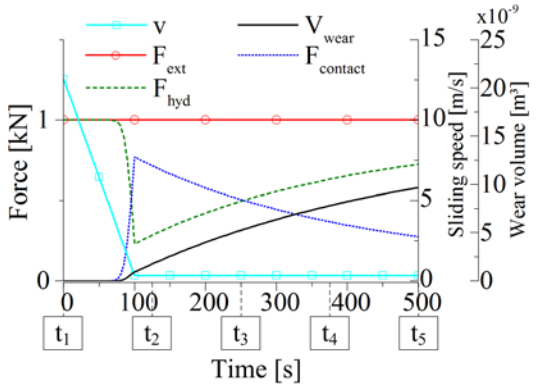

Figure 10. Resulting force equilibrium and run of wear volume in scenario 2.

The corresponding locally and chronologically resolved evolution of wear height is shown in fig. 11. Starting at initially 0 wear height the extend of the wear zone increases steadily with consecutive time. At the top of the journal bearing specimen wear occurs more intense.

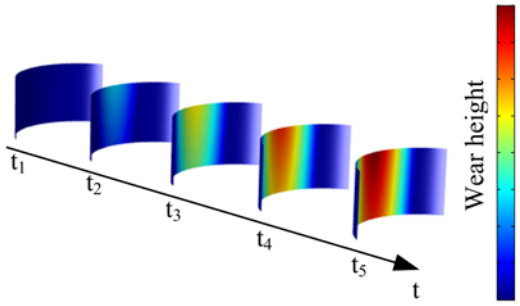

Figure 11: Chronologically and locally resolved wear height resulting from scenario 2.

6. Discussion

Considering scenario 1 the working principle of the developed numerical wear assessment methodology can be visualized. During initial loading the external load is carried by the hydrodynamic force. With increasing load the film thickness is decreased steadily. When the film thickness reaches the order of surface asperities at approx. 40 seconds the hydrodynamic carrying capacity is exceeded. The contact model starts to act leading to a solid contact force. Since the wear law is directly linked with solid contact pressure the wear volume starts to rise. When the tribological system switches between mixed and fluid friction the wear mechanism shows the desired behavior. In situation when solid contact occurs the wear volume further increases while staying at a constant level when both surfaces are completely separated by a lubrication film when the hydrodynamic force acts solely.

The results of scenario 2 show a decreasing $F_{contact}$ with consecutive time after establishing the desired mixed friction state. This scenario represents a running in process which is widely used in real applications. The system is set into an intense mixed friction state with a high solid contact share. The subsequent point of operation is in general situated in fluid friction regime. Hence this method is generally practiced to reach an energy optimized state ensuring low frictional losses and sufficient security against solid

contact and subsequent seizure failure. Due to the resulting wear pattern the surfaces adjust to each other supporting the hydrodynamic pressure build up. Having a look on the resulting wear pattern it is striking that wear doesn't occur constantly over the bearing height as might be expected. Even if the system is subjected to low loads in comparison with the stiffness of the specimen holder the displacement is large enough to cause a variation in the resulting film thickness leading to uneven wear pattern. If the numerical wear pattern in fig. 12 is compared to the wear pattern of a conducted test a good agreement can be stated.

Figure 12: Comparison of calculated wear pattern and the resulting wear pattern of a conducted test.

7. Conclusion

The numerical investigation of wear processes with the help of COMSOL Multiphysics® in lubricated systems reveals following points:

- By using an ODE wear equations can be implemented in COMSOL straightforwardly.
- The time dependent ODE allows a chronological and local solution of the wear process.
- Via a direct coupling to other used modules – in this case the coupling between Thin-Film Flow, Shell interface and wear equation – proceeding wear can directly be considered in the numerical analysis.
- Since in general fluid film heights are in µm-range the consideration of elastic deformations even at low loads and high stiffness of the surrounding structure is important to be able to evaluate resulting wear.

Achieved results are traceable and coincide with experiences of experimental data and practical use. Simulations work numerically stabile. At high wear depths it might be necessary to adjust solver settings slightly. In general the results depict a good agreement with test data qualitatively and a good suitability for using the developed numerical methodology as a wear assessment tool for generally lubricated contacts with wear resulting from arbitrary solid contact.

For qualitative statements it is necessary to take fluid properties into account properly, implement a suitable contact model and use significant wear coefficients.
However, by the use of appropriate wear laws also e.g. corrosive, erosive or cavitation wear can be implemented and numerically investigated with the help of the described wear assessment methodology in COMSOL Multiphysics®.

8. References

1. Regulation (EC) No 443/2009 of the European Parliament and of the Council of 23 April 2009 setting emission performance standards for new passenger cars as part of the Community's integrated approach to reduce CO 2 emissions from light-duty vehicles**.** *OJ L 140, 5.6.2009*

2. Priest, M., Taylor, C.M., Automobile engine Tribology – approaching the surface, *Wear*, **241**, 193-203 (2000)

3. Bergmann, P. et al. , Tribological Investigations of Journal Bearings by Means of a Close to Component Test Methodology, *Proceedings of Symposium der ÖTG*, 113-121 (2014)

4. Taylor, C.M., Automobile engine Tribology – design considerations for efficiency and durability, *Wear*, **221,** 1-8 (1998)

5. Reynolds, O. On the Theory of Lubrication and its Application to Mr. Beauchamp Tower's Experiments, including an Experimental Determination of the Viscosity of Olive Oil, *Philosophical Transactions of the Royal Society, Part I*, 228-310 (1886)

6. Greenwood, J.A., Williamson, J.B.P., Contact of Nominally Flat Surfaces, Proceedings of the Royal Society London, **295**,300-319 (1966)

7. Elabbasi, N., Simulating Wear in COMSOL Multiphysics, COMSOL Conference 2014, Boston

8.Sutton, D. et al., Simulation of Wear using LiveLink™ for MATLAB®, COMSOL Conference 2013, Rotterdam

9. Brown, S et al., Simulation solves the mystery behind an elevator accident, COMSOL News, 34-35 (2015)

10. Bergmann, P, Wear Evaluation of Journal Bearings, Manuscript in preparation (2016)

9. Acknowledgements

Financial support by the Austrian Federal Government (in particular from Bundesministerium für Verkehr, Innovation und Technologie and Bundesministerium für Wissenschaft, Forschung und Wirtschaft) represented by Österreichische Forschungsförderungsgesellschaft mbH and the Styrian and the Tyrolean Provincial Government, represented by Steirische Wirtschaftsförderungs-gesellschaft mbH and Standortagentur Tirol, within the framework of the COMET Funding Programme is gratefully acknowledged.

The authors like to give special thanks for support and enriching discussions to Miba Gleitlager GmbH.